Science Advances
AAAS

Supplementary Materials for

CHI3L1 signaling impairs hippocampal neurogenesis and cognitive function in autoimmune-mediated neuroinflammation

Wei Jiang *et al.*

Corresponding author: Changyong Tang, tangchy23@mail.sysu.edu.cn; Wei Qiu, qiuwei120@vip.163.com; Yu-Wen Alvin Huang, alvinhuang@brown.edu; Yaxiong Cui, cuimarcus@mail.tsinghua.edu.cn

Sci. Adv. **9**, eadg8148 (2023)
DOI: 10.1126/sciadv.adg8148

The PDF file includes:

Other Supplementary Material for this manuscript includes the following:

SUPPLEMEMTARY MATERIALS and METHODS

Primary astrocyte culturing and treatments

First, the whole brains from neonatal mouse pups (wildtype, C57BL/6) at postnatal day 0 (P0) were dissected out on ice. After removal of the meninges, the brains were washed in cold DMEM-F12 (C11330500BT, GIBCO) supplemented with 10% FBS (ST30-3302, PANTM SERATECH) and 1% penicillin streptomycin (15140-122, GIBCO). The brains were transferred to 0.25% trypsin EDTA for 20 minutes, and then DMEM-F12 complete medium was used to stop the trypsinization. Cell debris and aggregates were removed by passing the single-cell suspension through a 40 μm nylon mesh. After 5 minutes of centrifugation at 1000 g, the single-cell suspension was collected and cultured with astrocyte medium: DMEM-F12 (C11330500BT, GIBCO) containing 10% FBS (ST30-3302, PANTM SERATECH), 1% NEAA, 1% penicillin streptomycin (15140-122, GIBCO), 1% glutamine (GIBCO, 25030-081) and 1 mM sodium pyruvate (S8636, Sigma) in T-75 flasks for 7 days. The cultures were then vigorously shaken in an orbital incubator shaker at 350 rpm and 37°C for 12 hours. Following agitation, all cells present in the culture medium were removed, and the remaining attached cells were sub-cultured with the medium being replaced every 2-3 days for one week. Primary astrocytes were plated onto poly-D-lysine-coated glass coverslips in 24-well plates at a density of $8x10^3$ cells per well and allowed to settle at 37 °C in a 5% CO_2 incubator for 24 hours.

Primary mouse neural stem cells (NSCs) isolation and culturing

In short, the anatomical structure of the dentate gyrus was visualized by a dissection microscope, carefully removed out of the hippocampal regions, and then subject to the enzymatic digestion by using the MACS neural tissue dissociation kit according to the manufacturer's protocol (130-092-628, MACS Miltenyi Biotec). One milliliter of trypsin inhibitor (S10088, Yuan Ye Biology) was added to each sample to stop digestion. After 5 minutes of centrifugation at 1000 g, the single-cell suspension was collected and cultured with the maintenance medium for proliferation (proliferation medium), formulated with neurobasal (21103049, GIBCO) medium containing 2% B27 supplement (17504044, GIBCO), 20 ng/mL basic fibroblast growth factor (FGF-2, K1606, PeproTech), 20 ng/mL epidermal growth factor (EGF, A2306, PeproTech), 1% penicillin streptomycin (15140-122, GIBCO) and 2 mM L-glutamine (25030-081, GIBCO) in a 5% CO_2 incubator at 37 °C. Without further description, half of the medium was replaced every 3 days. To assay the NSC proliferation, 24 hours after plating, the cells were incubated with the indicated vehicle controls or biological reagents for 3 days, and then the EdU from a Cell Proliferation Kit was administered according to the manufacturer's protocol (C0078L, Beyotime). For the assays of neuronal differentiation, 48 hours after plating, the cells were changed to the differentiation medium composed of neurobasal medium containing 2% B27 supplement (17504044, GIBCO), 1% penicillin streptomycin (15140-122, GIBCO) and 2 mM L-glutamine (25030-081, GIBCO), with the co-incubation of the indicated vehicle controls or biological reagents.

Immunoblotting and the densitometric analysis

Cell lysates were derived from primary mouse astrocytes or NSCs using radioimmunoprecipitation assay (RIPA) lysis buffer. The proteins were separated on 8-15% sodium dodecyl sulfate-polyacrylamide gels by electrophoresis and then transferred to methanol-activated polyvinylidene fluoride (PVDF) membranes. The membranes were blocked in 5%

defatted milk powder for 1 hour at 37 °C and incubated with primary antibodies overnight at 4 °C. The membranes were then washed three times with TBST and incubated with horseradish peroxidase (HRP) secondary antibodies for 1 hour. Protein bands were visualized with Millipore ECL Plus reagent and imaged on a Tanon 5500 Imaging Analysis System.

Immunohistochemistry for confocal imaging of mouse hippocampal slices

Mice were euthanized by intraperitoneal injection of 2% pentobarbital sodium and given an initial flush with 0.01 M phosphate buffered saline (PBS). Then, the mice were transcardially perfused with 4% PFA. Mouse brains were fixed in 4% PFA at 4°C overnight and then placed in 30% sucrose until submerged. The brains were cut into 40-μm-thick sections coronally using a microtome and placed in a 96-well plate. The slices were kept in cryoprotectant solutions (glycerol, ethylene glycol and 0.1 M phosphate buffer, pH 7.4, 1:1:2 by volume) at 4 °C. For immunofluorescence staining, floating sections were blocked with 300 μL donkey or goat serum and 250 μL 10% Triton X-100 per 10 mL PBS for 1 hour at room temperature and then sequentially incubated with primary antibodies overnight at 4°C. The sections were washed with PBS three times, and then incubated with the secondary antibody at room temperature for 1 hour. The nuclei were then stained with 4',6-dimethyl-2'-phenylindole dihydrochloride (DAPI, 2261b, Sigma Aldrich). The images were observed under a laser confocal microscope. Each group of immunohistochemical experiments was repeated at least 3 times. For DCX or Sox2 staining, antigen retrieval was needed. Antigen retrievals were performed in citrate buffer (pH 9.0) with a microwave for 10 minutes at 95 °C followed by 20 minutes of cooling at room temperature.

Sequences of the primers for quantitative real-time PCR (qPCR)

The sequences of the forward (F, 5'-3') and reverse (R, 5'-3') primers for the individual genes:

1. IL1α, F: CAGTGAGACCTTCACTGAAG, R: CTGGAAGTCTGTCATAGAGG
2. IL1β, F: GGCTGCTTCCAAACCTTTGA, R: GCTGTTGATGGACCTACAGGA
3. IL2, F: GCTGTTGATGGACCTACAGGA, R: TTCAATTCTGTGGCCTGCTT
4. IL4, F: CATCGGCATTTTGAACGAG, R: ACGTTTGGCACATCCATCTC
5. IL5, F: GACCTTGACACAGCTGTCCG, R: AGCATTTCCACAGTACCCCC
6. IL6, F: GCTTAATTACACATGTTCTCTGGGAAA, R: CAAGTGCATCATCGTTGTTCATAC
7. IL18, F: TCCAACTGCAGACTGGCAC, R: GGCAGGAGTCCAGAAAGCAT
8. TNF-α, F: GACTCAAATGGGCTTTCCGA, R: TCCAGCCTCATTCTGAGACAGAG
9. TNF-β, F: AACCTGCTGCTCACCTTGTT, R: CAGTGCAAAGGCTCCAAAGA
10. NFκB, F: CATGAAGCAGCTGACAGAAG, R: TTCAATAGGTCCTTCCTGCC
11. CCL2, F: TGAGTAGGCTGGAGAGCTACAAG, R: TGTATGTCTGGACCCATTCCTTC
12. CCL5, F: CCTCACCATCCTCACTG, R: TCTTCTCTGGGTTGGCACAC
13. CCL6, F: GGCCCAAGATCTGGGAACAA, R: CTCTATTGTGGCAGGGCGAA
14. CCL7, F: ATCTCTGCCACGCTTCTGTG, R: CCTCTTGGGGATCTTTTGTTT
15. CCL11, F: GGCTTCATGTAGTTCCAGAT, R: CCATTGTGTTCCTCAATAATCC
16. CCL17, F: TGCTTCTGGGGACTTTTCTG, R: GAATGGCCCCTTTGAAGTAA
17. CCL20, F: ATGGCCGATGAAGCTTGTGA, R: CTCCTTGGGCTGTGTCCAAT
18. CCL22, F: TCTTGCTGTGGCAATTCAGA, R: GAGGGTGACGGATGTAGTCC
19. CXCL1, F: TAGGGTGAGGACATGTGTGG, R: AAATGTCCAAGGGAAGCGT
20. CXCL2, F: GGAAGCCTGGATCGTACCTG, R: TGAAAGCCATCCGACTGCAT

21. CXCL5, F: GCCCTACGGTGGAAGTCATA, R: GTGCATTCCGCTTAGCTTTC
22. CXCL10, F: CATCCCTGCGAGCCTATCC, R: CATCTCTGCTCATCATTCTTTTTC
23. CHI3L1, F: GGCAAGAAGCAAGACGTAGG, R: CAGACCAGCTTGTACGCAGA
24. GFAP, F: CATGCCACGCTTCTCCTTGT, R: ATCATCTCTGCACGCTCGCT
25. ALDH1L1, F: GGGGACAGGAGGGTGCTAAGTC, R: TGTCATCCCCTGGAACTATCCC
26. S100β, F: AGCTGGAGAAGGCCATGGTG, R: GAACTCGTGGCAGGCAGTAG
27. IBA1, F: TGAGGAGCCATGAGCCAAAG, R: GCTTCAAGTTTGGACGGCAG
28. Tmem119, F: CCTTCACCCAGAGCTGGTTC, R: GGCTACATCCTCCAGGAAGG
29. CX3CR1, F: CACCAAAGCCAGCACATAGGAGAG, R: GTCTGCGGATCTTGGACAAACAAATG

Sequences of the validated shRNAs

The shRNA sequences used to knock down CHI3L1 receptors are:

1. CRTH2-shRNA_1: CCGGGCTCAACACAATACCATATTTCTCGAGAAATATGGTATTGTGTTGAGCTTTTTT
2. CRTH2-shRNA_2: CCGGCACTGCTCTATGTGTTCACATCTCGAGATGTGAACACATAGAGCAGTGTTTTTT
3. TMEM219-shRNA_1: CCGGGTCGGCTTACTGACCACTTTGCTCGAGCAAAGTGGTCAGTAAGCCGACTTTTTT
4. TMEM219-shRNA_2: CCGGCATGGTAGTCAGATAGGATTGCTCGAGCAATCCTATCTGACTACCATGTTTTTT
5. IL-13Rα2-shRNA_1: CCGGATATTCTGATACCAACTATACCTCGAGGTATAGTTGGTATCAGAATATTTTTTT
6. IL-13Rα2-shRNA_2:
7. CCGGTTGGACTCATCAGACTATAAACTCGAGTTTATAGTCTGATGAGTCCAATTTTTT

Production of lentivirus and adeno-associated virus (AAV) particles

The lentivirus and AAV preparations were routinely produced the transfection of human embryonic kidney (HEK293T; RRID:CVCL_0063) cells with the desired vectors. The sequences of the shRNAs targeting against the test CHI3L1 receptors are listed in a table included in the Supplemental Materials. In summary, the HEK293T cells were maintained at 37°C in a CO2 cell incubator (Thermo Fisher 371) in Dulbecco's Modification of Eagle's Medium (DMEM) 1× (MOD.) (319-005-CL, MULTICELL) containing 10% fetal bovine serum (ST30-3302, PANTM SERATECH), 1% penicillin streptomycin (15140-122, GIBCO), and 1% glutamine (GIBCO, 25030-081) and passaged every 2-3 days with 0.05% trypsin EDTA. For the production of lentivirus particles, the designed and cloned lentiviral vectors were co-transfected with helper plasmids psPAX and pMD2G into HEK293T cells using polyethyleneimine (PEI, PR40001, Proteintech Group). The culture medium was changed within 4 hours. The medium containing lentivirus was collected at 2-4 days post transfection, filtered, and concentrated by

ultracentrifugation (Beckman SW32 Ti). The viruses were washed once with PBS and then resuspended in 200 μL PBS. Each virus tube was labeled and stored at -80°C. As for the AAV, the package with AAV-DJ capsids were used for the intended high efficiency of *in vivo* infection. AAV vectors with pHelper and pRC-DJ were transfected into HEK293 cells, which were collected and lysed 72 hr later. The virus preparations were concentrated from cell lysates by fractioning with iodixanol gradient (40%) and filtering with 100,000 MWCO tube filter. For both lentivirus and AAV production, the virus titer was measured by transducing HEK293 with a series of dilutions and analyzing the fluorescent signal from the co-expressed eGFP. Before the concentration, the typical titer was among the range of ≒10^7 transduction units (TU) ml before the concentration.

Animal care and genotyping by the genomic DNA extraction and PCR

Overall, the 8-week-old wildtype (C57BL/6, Charles River) and the CHI3L1-floxed transgenic mice (*Chil1*$^{f/f}$, Cyagen Biosciences) were used for the described experiments, and maintained for additional four to eight weeks according to the individual study design. These mice were placed in the animal facility of Guangdong Laboratory Animals Monitoring Institute under a 12-hour light/dark cycle constantly under 22-26°C and 50%–60% humidity. The mice could obtain food and water in the cage *ad libitum*. *Chil1*$^{f/f}$ mice were created by Cyagen Biosciences (NCBI: 12654). All mice in the study were backcrossed to the C57BL/6 background for at least six generations. The animals were randomly assigned to the experimental group. Before the experiment was completed, the experimenter did not know the identities of the animals. Adult neural stem cells were isolated from eight- to twelve-week-old WT mice. All procedures and feeding were carried out in accordance with the scheme approved by the Laboratory Animals Monitoring Institute and the animal experiment ethics committee of the Third Affiliated Hospital of Sun Yat-Sen University. No mice were used in other research projects. The influence of sex was not evaluated in this study. For the extraction of genomic DNA, mouse tails were digested overnight in 200 mL lysis solution (containing 1 mg/mL proteinase K, 50 mM Tris-HCl pH 8.0, 100 mM EDTA, 100 mM NaCl and 1% SDS) at 55 °C. Four hundred milliliters of NaCl (6 M) were added to each sample and the solution was mixed well. The solution was incubated on ice for 10 minutes. The samples were centrifuged at 13,000 rpm for 10 minutes at room temperature. The supernatant was transferred to a new 1.5 mL centrifuge tube with 800 mL ethanol (70% in ddH2O) and mixed well. The samples were centrifuged at 13,000 rpm for 10 minutes. The genomic DNA pellet was dissolved in 200 mL TE buffer (10 mM Tris-HCl, 1 mM EDTA, pH 8.0). Genotyping was performed with PCR-based assays using genomic DNA. The sequences of the primers used were: the forward primer (5'-3'), GCTACCCAACATGTCAATAGCTCA; the reverse primer (5'-3'), CATATGGTGGGCAATAATCTTGGA.

Open Field Test

The Open Field Test by experienced experimenters to detect the locomotor activity and exploratory behavior of mice in a standardized manner. Mice of different experimental groups were placed in a 50 cm x 50 cm x 50 cm arena and allowed to explore the site freely for 10 minutes. After the test, they were placed back in their cage. The distance traveled was recorded to evaluate the motor ability of the mice, and the time spent in the central area was measured to detect the anxiety of the mice. Experimenters were blinded to the genotypes and mice.

Morris Water Maze

The Morris Water Maze task was performed as previously described. Briefly, the MWM test consisted of a water-filled pool (diameter 120 cm) with a hidden escape platform under the water surface. The platform (10 cm wide) was located approximately 1 cm below the water level and was divided into four quadrants. The MWM is divided into training and testing phases. In the training phase, mice were randomly placed in the water maze from four different starting positions (NE, NW, SE and SW). The mice were trained for five days to find the hidden platform. After taking the mouse out of the maze, the water on the mouse was wiped with a towel and then the mouse was placed back in the cage. After 24 hours of visual platform training, a detection test was conducted, during which the platform was removed and times crossing the platform area were measured by camera to test short-term spatial memory. All tests were performed at the same time every day. Experimenters were blinded to the genotypes and mice.

Production of lentivirus and adeno-associated virus (AAV) particles

The lentivirus and AAV preparations were routinely produced the transfection of human embryonic kidney (HEK293T) cells with the desired vectors. The sequences of the shRNAs targeting against the test CHI3L1 receptors are listed in a table included in the Supplemental Materials. In summary, the HEK293T cells were maintained at 37°C in a CO2 cell incubator (Thermo Fisher 371) in Dulbecco's Modification of Eagle's Medium (DMEM) 1× (MOD.) (319-005-CL, MULTICELL) containing 10% fetal bovine serum (ST30-3302, PANTM SERATECH), 1% penicillin streptomycin (15140-122, GIBCO), and 1% glutamine (GIBCO, 25030-081) and passaged every 2-3 days with 0.05% trypsin EDTA. For the production of lentivirus particles, the designed and cloned lentiviral vectors were co-transfected with helper plasmids psPAX and pMD2G into HEK293T cells using polyethyleneimine (PEI, PR40001, Proteintech Group). The culture medium was changed within 4 hours. The medium containing lentivirus was collected at 2-4 days post transfection, filtered, and concentrated by ultracentrifugation (Beckman SW32 Ti). The viruses were washed once with PBS and then resuspended in 200 μL PBS. Each virus tube was labeled and stored at -80°C. As for the AAV, the package with AAV-DJ capsids were used for the intended high efficiency of *in vivo* infection. AAV vectors with pHelper and pRC-DJ were transfected into HEK293 cells, which were collected and lysed 72 hr later. The virus preparations were concentrated from cell lysates by fractioning with iodixanol gradient (40%) and filtering with 100,000 MWCO tube filter. For both lentivirus and AAV production, the virus titer was measured by transducing HEK293 with a series of dilutions and analyzing the fluorescent signal from the co-expressed eGFP. Before the concentration, the typical titer was among the range of $\fallingdotseq 10^7$ transduction units (TU) ml before the concentration.

Material availability Statement

The newly created materials would be available for sharing, made with no more restrictive terms than in the Uniform Biological Material Transfer Agreement (UBMTA) or an equivalent form of agreement and without reach through requirements.

SUPPLEMEMTARY FIGURES

Supplementary Figure 1

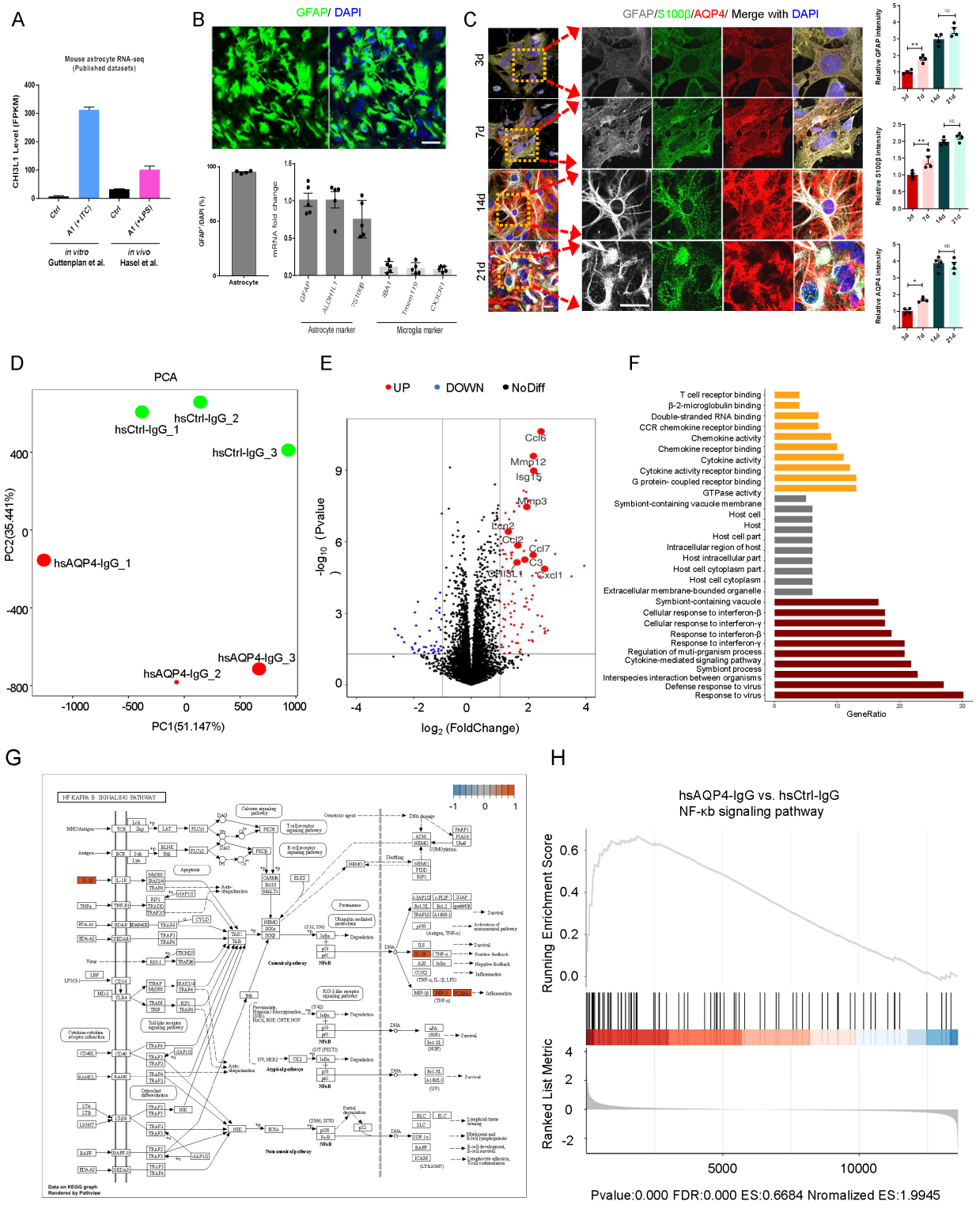

Fig. S1 Additional data of transcriptional analyses on mouse astrocytes activated by pro-inflammatory stimuli.

(**A**) Evaluation of CHI3L1 induction in neuroinflammation by meta-analyses of published astrocyte transcriptomic datasets on wildtype mouse astrocytes, in primary cultures treated with pro-inflammatory cytokines IL-1α, TNF and C1q (ITC for 24h; '*in vitro*'), or in acutely purified astrocytes from mice stimulated by intraperitoneal injection of liposaccharide (LPS after 24h; '*in vivo*'), based on the bulk RNA-Seq datasets from Guttenplan *et al*. (*41*) and Hasel *et al*. (*40*)

(**B**) Assessment of the purity in the cultures of primary mouse astrocytes. Top, representative images of immunostaining to label all cells (DAPI, blue) and the cells positive for astrocyte marker (GFAP, green) in 14-day-old cultures as in **Fig. 1**. Left bar graph, the percentage of the cultured cells positive for the astrocyte marker (GFAP/DAPI, ~100%) n=4 independent batches of astrocyte cultures. Right bar graph, the expression of multiple markers genes for astrocytes (GFAP, ALDH1L1 and S100β) and microglia (IBA1, Tmem119 and CX3CR1) by individual qPCRs on astrocyte cultures (normalized to the loading control GAPDH and plotted relative to GFAP=1.0; DIV 14), showing a minimal amount of microglia present in the primary cultures of mouse astrocytes. Scale bar, 50 μm. n=5 independent experiments.

(**C**) The characterization of astroglial development *in vitro*, by assaying the expression of marker genes with immunostaining (GFAP, gray; S100β, green; AQP4, red), which plateaued on DIV14 (14d) to indicate functional maturity. Scale bar, 20 μm n=4 batches of cultures.

(**D**) Functional principal component analysis (PCA) of bulk RNA-Seq from this study on primary mouse astrocytes treated with hsCtrl-IgG or hsAQP4-IgG, 100 ng/ml for 24h.

(**E**) Volcano plot of gene fold changes induced by hsAQP4-IgG as compared to the hsCtrl-IgG stimulation from this study. p value<0.05 and a fold change cutoff of log2 ratio≥0.5 were used to detect the differentially expressed genes (DEGs, a total of 152). Red dots, 110 upregulated genes; blue dots, 42 downregulated genes. The exemplary secreted protein genes overlapped with the published dataset of Walker-Caulfield *et al.* (*37*) were indicated.

(**F**) GO enrichment analysis of the 152 DEGs between primary astrocytes treated with hsCtrl-IgG or hsAQP4-IgG from this study.

(**G**) The NFκB canonical pathway was identified via the pathway visualization of the 91 overlapped DEGs (**Fig. 1F-J**) by extracting the Kyoto Encyclopedia of Genes and Genomes database (KEGG) with the data integration tool of Pathview.

(**H**) The Gene Set Enrichment Analysis (GSEA) of the 91 overlapped DEGs (**Fig. 1F-J**), showing the expression of the NFκB pathway gene set was statistically enriched in the hsAQP4-IgG-treated astrocytes, as compared to the control of hsCtrl-IgG treatment.

The bar graphs of (B) and (C) were presented as the mean ± SEM; the statistical evaluation of (C) was performed with one-way ANOVA and Tukey's post hoc multiple comparisons (only selected comparisons shown here). *p < 0.05, **p<0.01, NS, not significant.

Supplementary Figure 2

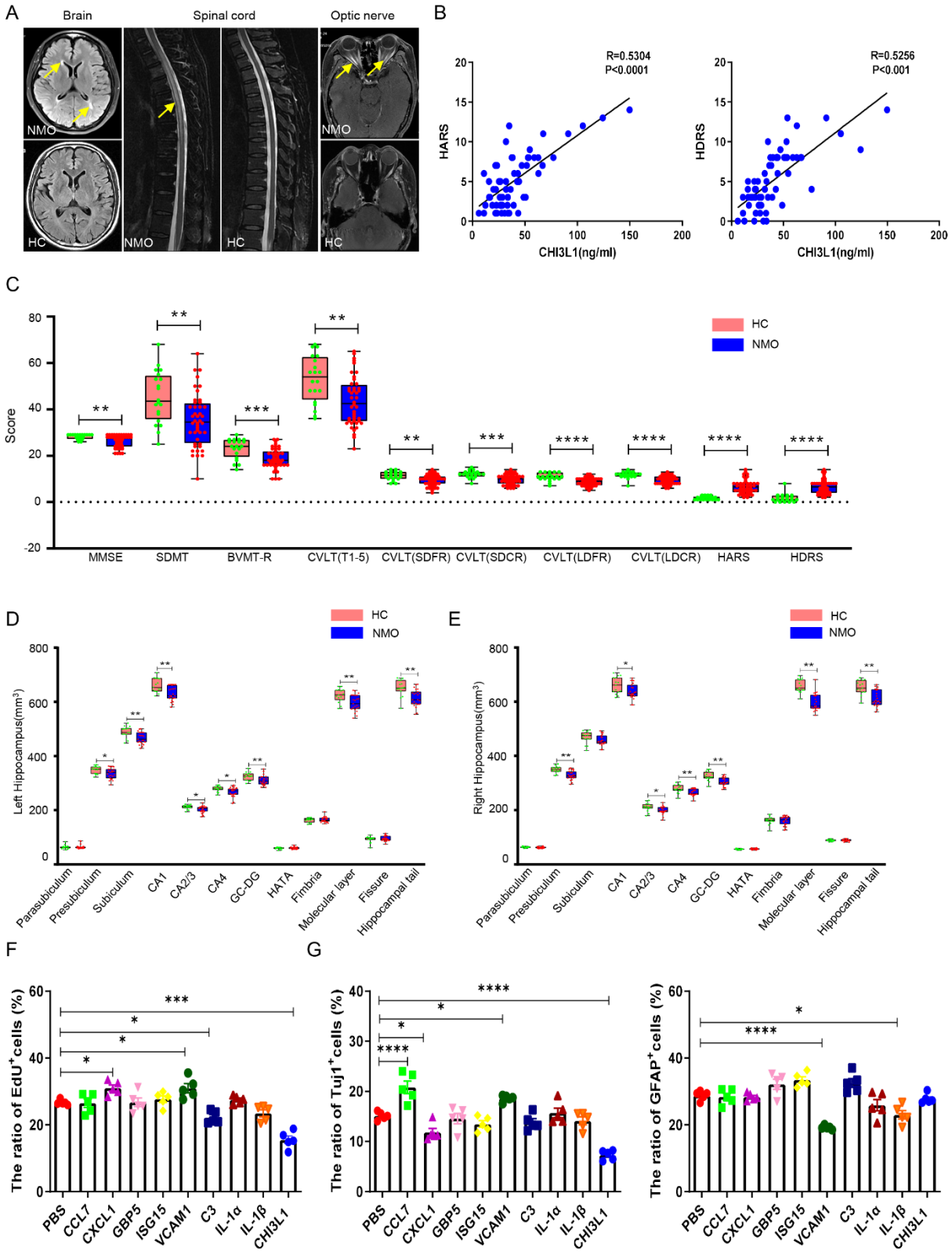

Fig. S2 Additional data of MRI scans and neuropsychological tests from health controls and NMO patients

(**A**) Representative MRI images of brain, spinal cord and optic nerve from healthy control (HC) subjects and NMO patients. The typical lesions of neuromyelitis and optic neuritis were indicated by the yellow arrows.

(**B**) In complementation to **Fig. 2C**, the positive correlation between the scores of HARS and HDRS (for anxiety- and depression-like symptoms) with serum CHI3L1 levels in NMO patients, plotted in linear regression. n=64.

(**C**) In complementation to **Fig. 2C,** the scoring of the neuropsychological tests in health control (HC) subjects and NMO patients, plotted in the box chart of distribution for the test actual scores. HC, n=20; NMO, n=44.

(**D**) The 3D size quantification of the hippocampal subfields on the left side for healthy control (HC) subjects and NMO patients. HC, n=15; NMO patients: n=23.

(**E**) The 3D size quantification of the hippocampal subfields on the right side for healthy control (HC) subjects and NMO patients. HC, n=15; NMO patients: n=23.

(**F-G**) The assessment of the effects from the secreted astroglial factors of neuroinflammation on the NSC proliferation and neuronal differentiation *in vitro*, similar as in **Fig. 2G**. The primary mouse NSC cultures were first stimulated with vehicle control of PBS or the recombinant proteins (100ng/mL) selected from (**Fig. 1H-J**), including CCL7, CXCL1, GBP5, ISG15, VCAM1, C3, IL-1α, IL-1β and CHI3L1, for 3 days in the proliferation media. EdU was administered in half of the treated cultures for 2 hours before the fixation and immuno-staining to evaluate the proliferation by the percentage of EdU^+ cells (F). The remaining half of the NSC cultures were switched into the differentiation media, being allowed to differentiate for additional 3 days with the incubation of PBS or the selected astroglial factors (100 ng/ml), and were then fixed and subject to confocal analyses for differentiation into mature $Tuj1^+$ neurons or $GFAP^+$ glial cells (G).

Data in (C-G) were presented as the mean ± SEM; in (B), (C-E) the statistical significance was evaluated with Student's t test for two-group comparisons (HC vs. NMO); in (F-H), one-way ANOVA was used with Tukey's post hoc multiple comparisons. Non-significant comparisons are not identified. *$p < 0.05$, **$p<0.01$, ***$p < 0.001$, ****$p < 0.001$.

Abbreviation: HC, healthy control. NMO, neuromyelitis optica. HARS, Hamilton Anxiety Rating Scale. HDRS, Hamilton Depression Rating Scale. MMSE, Mini-Mental State Examination. SDMT, Symbol Digit Modalities Test. BVMT-R. Brief Visuospatial Memory Test Revised. CVLT (T1-5), California Verbal Learning Test (Trial 1-5). CVLT-SDFR: California Verbal Learning Test Short Delayed Free Recall. CVLT-SDCR, California Verbal Learning Test Short Delayed Cue Recall. CVLT-LDCR), California Verbal Learning Test Long Delayed Cue Recall. CVLT-LDFR, California Verbal Learning Test Long Delayed Free Recall. GC-DG, granule cell layer of the dentate gyrus. HATA, hippocampal amygdala transition area.

Supplementary Figure 3

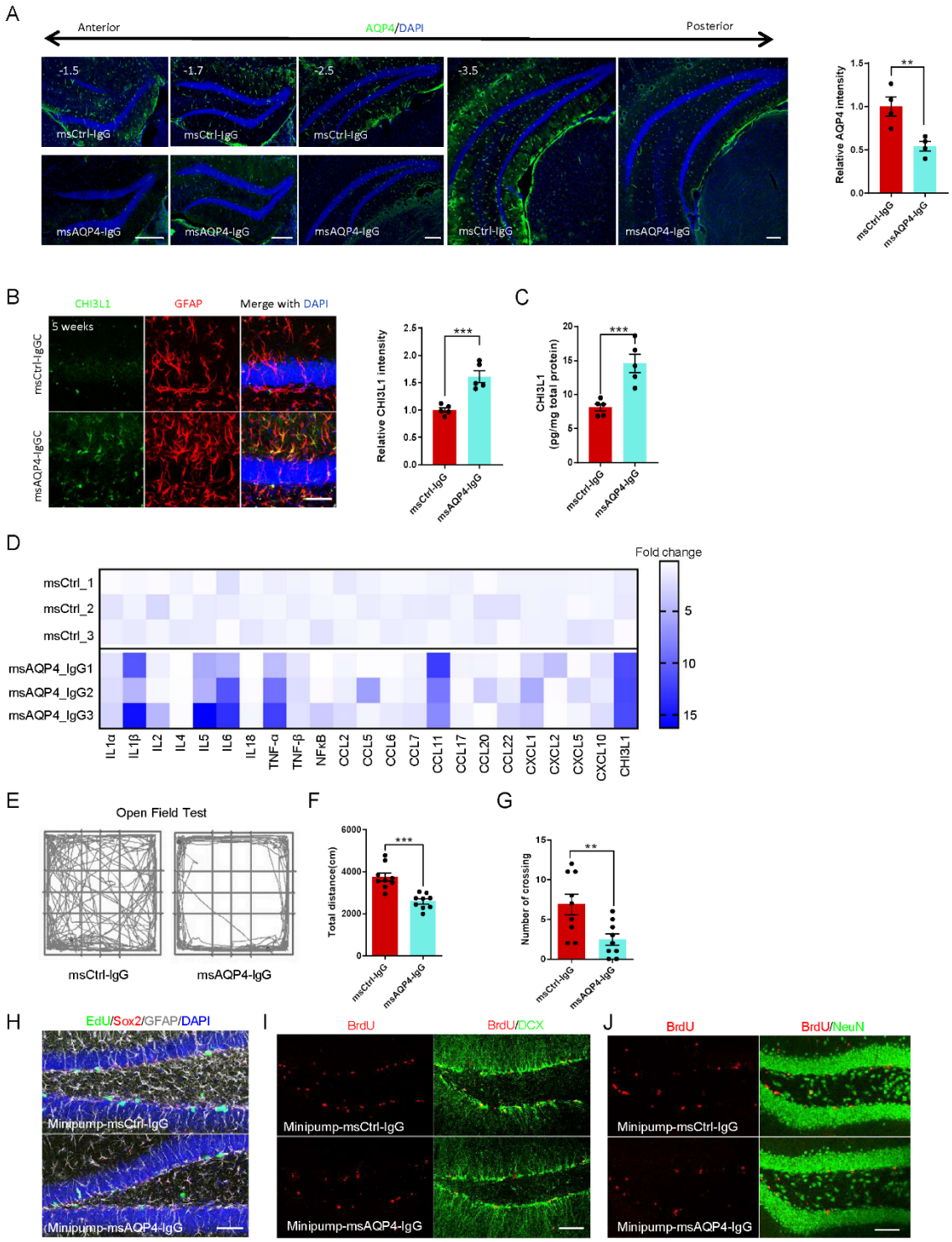

Fig. S3 Additional data for the biochemical, histopathological and behavioral assays on the mice receiving msCtrl-IgG or msAQP4-IgG.

(**A**) The examination of the anti-AQP4 IgG effect, assayed by the loss of AQP4 expression in the vicinity of the injection site (relative to bregma, -1.5 ~ -3.5 mm) within the dentate gyrus. Bar graph, the AQP4 immunofluorescent signal (green) was significantly reduced in the hippocampal sections within the 1 mm distance from the injection site. The same range was used for our analyses of the NSC proliferation and neuronal differentiation of NSCs. Scale bar, 100 μm.

(**B**) Assessment of the lasting CHI3L1 expression in astrocytes induced by msAQP4-IgG after an interval of 5 week (relevant to **Fig. 3D**), quantified by the intensity of CHI3L1 fluorescence (green) that was colocalized with GFAP signals (red) and presented as the relative levels after setting the value of msCtrl-IgG as 1.0. n=5 animals per group. Scale bar, 50 μm.

(**C**) Measurements of CHI3L1 levels by ELISA on the lysates of acutely dissected, unfixed hippocampal tissues from the mouse brains stereotaxically injected with msCtrl-IgG- or msAQP4-IgG-treated, complementing the immune-staining results of CHI3L1 induction by msAQP4-IgG in Fig. 3D. n=3 animals per group.

(**D**) Examinations of the pro-inflammatory genes induced upon astroglial activation by msAQP4-IgG in the hippocampal lysates as in fig. S3A. The data of qPCR assays on the cytokines and chemokines including those identified by the RNA-seq (**Fig. 1H-J**) were plotted as the heatmap of gene fold change. Dark blue indicated no change and white color indicated >10-fold chance. n=3 animals per group.

(**E**) The mice stereotaxically injected with msCtrl-IgG or msAQP4-IgG went through the standardized open field test before the Morris water maze to evaluate their overall locomotor activities and anxiety-like behaviors, with their representative movement paths shown here.

(**F** and **G**) Quantification of the open field test results by measuring the average total distance travelled (**F**) and the average crossing numbers through the center area (**G**). n=9 mice per group.

(**H**) Representative confocal images for the analyses of NSC proliferation, complementing the results in **Fig. 3M-O**. The labeling of EdU (green), Sox2 (red), GFAP (gray) and DAPI (blue) was to identify the total proliferating cells (EdU^+), the radial glia-like cells ($EdU^+GFAP^+Sox2^+$), and the transiently amplifying progenitor-like cells ($EdU^+GFAP^-Sox2^+$). Scale bar, 100 μm.

(**I**) Representative confocal images of labeling the newborn immature neurons in the hippocampus SGZ from mice injected with msCtrl-IgG or msAQP4-IgG, complementing the results in **Fig. 3P.** BrdU was immune-stained in red and the immature neuronal marker DCX in green. Scale bar, 100 μm.

(**J**) Representative confocal images of labeling the mature neurons newly differentiated from NSCs in the hippocampus SGZ as in fig. S3J, complementing the results in **Fig. 3Q**. BrdU was immune-stained in red and the mature neuronal marker NeuN in green. Scale bar, 100 μm.

Data in (B), (C) and (F-G) were presented as the mean ± SEM in bar graphs, and the statistical significance was evaluated with Student's t test for two-group comparisons. $*p < 0.05$, $**p<0.01$, $***p < 0.001$.

Supplementary Figure 4

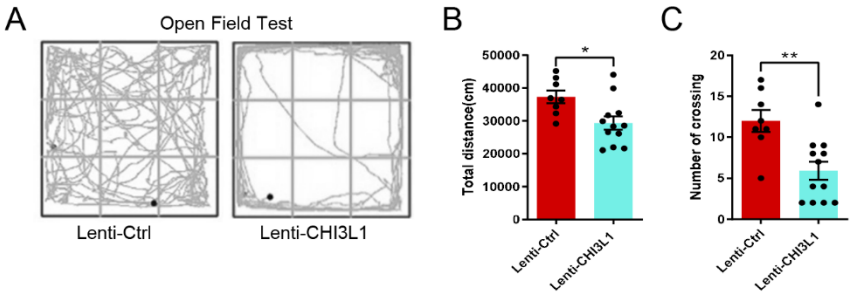

Fig. S4 Additional data on the behavioral consequences of the CHI3L1 over-expression

(**A**) The open field test was performed prior to Morris water maze at week 4-6 (Fig. 4B) to evaluate the locomotor activities and anxiety-like behaviors in mice lentivirally transduced to over-express eGFP (Lenti-Ctrl) or CHI3L1 plus eGFP (Lenti-CHI3L1). Representative movement paths of both groups were shown here.

(**B** and **C**) Quantification of the open field test by measuring the total travel distances (B) and the crossing numbers through the center area (C) of both groups. Lenti-Ctrl, n=8 mice; Lenti-CHI3L1, n=12.

Data in (B and C) are presented as the mean ± SEM; Data in (B and C) statistical significance was evaluated with unpaired one-tailed Student's t test for two group comparisons. *$p < 0.05$, **$p<0.01$.

Supplementary Figure 5

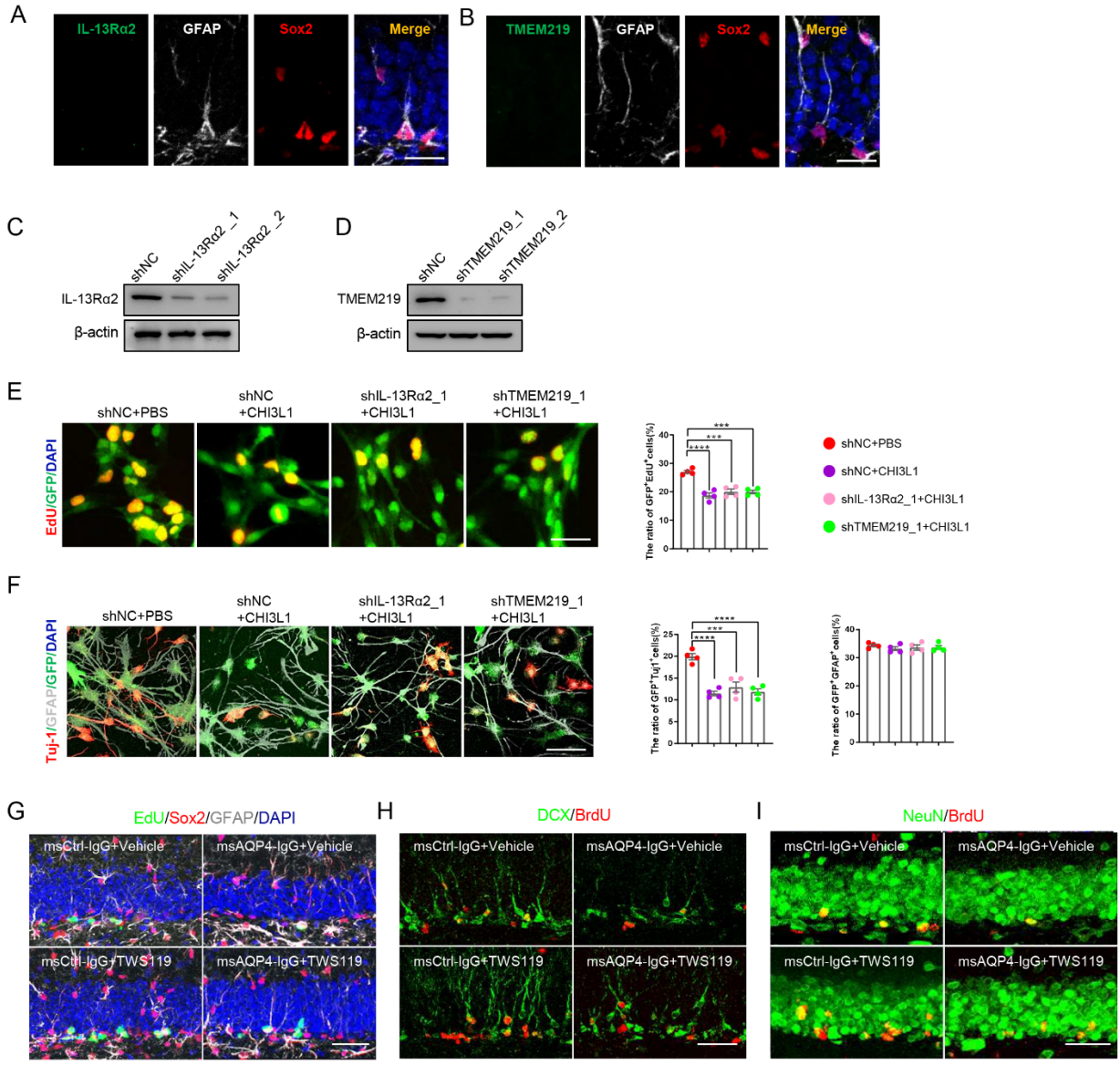

Fig. S5 The knockdown of CHI3L1 receptors IL-13Rα2 and TMEM219 did not affect the inhibitory CHI3L1 signaling for NSC proliferation and differentiation

(**A**) Little expression of IL-13Rα2, a common CHI3L1 receptor for immune cells, in NSCs within the SGZ of dentate gyrus from 8-week-old wildtype mice, assayed by immunostaining of IL-13Rα2 (green) and the radial glia-like NSC markers Sox2 (red) and GFAP (white) plus the nuclear marker DAPI (blue). This confocal imaging complemented Fig. 5B. Scale bars, 20 μm.

(**B**) Very low level of CHI3L1 receptor TMEM219 in NSCs within the SGZ of dentate gyrus, assayed by immunostaining of IL-13Rα2 (green) and the radial glia-like NSC markers Sox2 (red) and GFAP (white) plus the nuclear marker DAPI (blue). This confocal imaging complemented **Fig. 5B**. Scale bars, 20 μm.

(**C**) The knockdown efficiency of 2 shRNAs targeting against IL-13Rα2, assayed by immunoblotting of cell lysates from NSCs transduced with lentiviruses to express the non-targeting control shRNA (shNC), shIL-13Rα2_1 or shIL-13Rα2_2 as described in **Fig. 5E and F**. β-actin served as the loading control.

(**D**) Relevant to **Fig. 5E and F,** the evaluation of TMEM219 knockdown efficiency by 2 shRNAs, shTMEM219-1 and shTMEM219_2, transduced in NSC cultures and compared to the protein levels of TMEM219 and β-actin.

(**E**) The knockdown of IL-13Rα2 or TMEM219 did not affect the inhibition of NSC proliferation by CHI3L1, in parallel to the experiments in **Fig. 5H**. The cultured mouse NSCs grown in proliferation medium were transduced to express shNC, shIL-13Rα2_1 or shTMEM219_1 and then treated with PBS or CHI3L1 (100 ng/ml). The EdU was added into the cultures two hours before the fixation and immune-staining. Left panels, representative confocal images of the indicated 4 groups. Right bar graphs, the quantification of NSC proliferation was plotted as the ratio of the proliferating cells (GFP^+ EdU^+) and total cells (GFP^+, co-expressed with shRNAs; ~100% colocalization with $DAPI^+$ cells) in cultures. n=4 experiments per group. Scale bars, 100 μm.

(**F**) In relation to **Fig. 5I**, the knockdown of IL-13Rα2 or TMEM219 did not affect the inhibition of NSC differentiation by CHI3L1. The mouse primary NSCs were cultured in the differentiation medium and transduced to express shNC, shIL-13Rα2_1 or shTMEM219_1, with the incubation of PBS or CHI3L1 (100 ng/ml) for 3 days. After fixation, the immuno-staining was performed to label essentially all cells with GFP (green) and DAPI (blue), the newly differentiated neurons with Tuj1 (red) and astroglial cells with GFAP (gray), in the panels of the representative images. The bar graphs were the quantification of neuronal differentiation, shown in the ratio of neurons and total cells (GFP^+Tuj1^+/GFP^+, left) and the ratio of astroglia and total cells (GFP^+GFAP^+/GFP^+, right). n=4 experiments. Scale bars, 100 μm.

(**G**) Representative images to complement **Fig. 5L-5N**, showing the mouse dentate gyrus sections labeled with EdU (green) and NSC markers Sox2 (red) and GFAP (gray). Scale bars, 50 μm.

(**H**) Representative images to complement **Fig. 5O and 5P**, showing the differentiation of BrdU-labeled NSCs into immature neurons, immunostained with BrdU (red) and DCX (green). Scale bars, 50 μm.

(**I**) Representative images to complement **Fig. 5Q**, showing the differentiation of BrdU-labeled NSCs into mature neurons, immunostained with BrdU (red) and NeuN (green). Scale bars, 50 μm.

Data in (E) and (F) were presented as the mean ± SEM and their statistical significance was evaluated with one-way ANOVA and Tukey's post hoc multiple comparisons. Non-significant comparisons are not identified. *$p < 0.05$, **$p<0.01$, ***$p < 0.001$, ****$p < 0.0001$.

Supplementary Figure 6

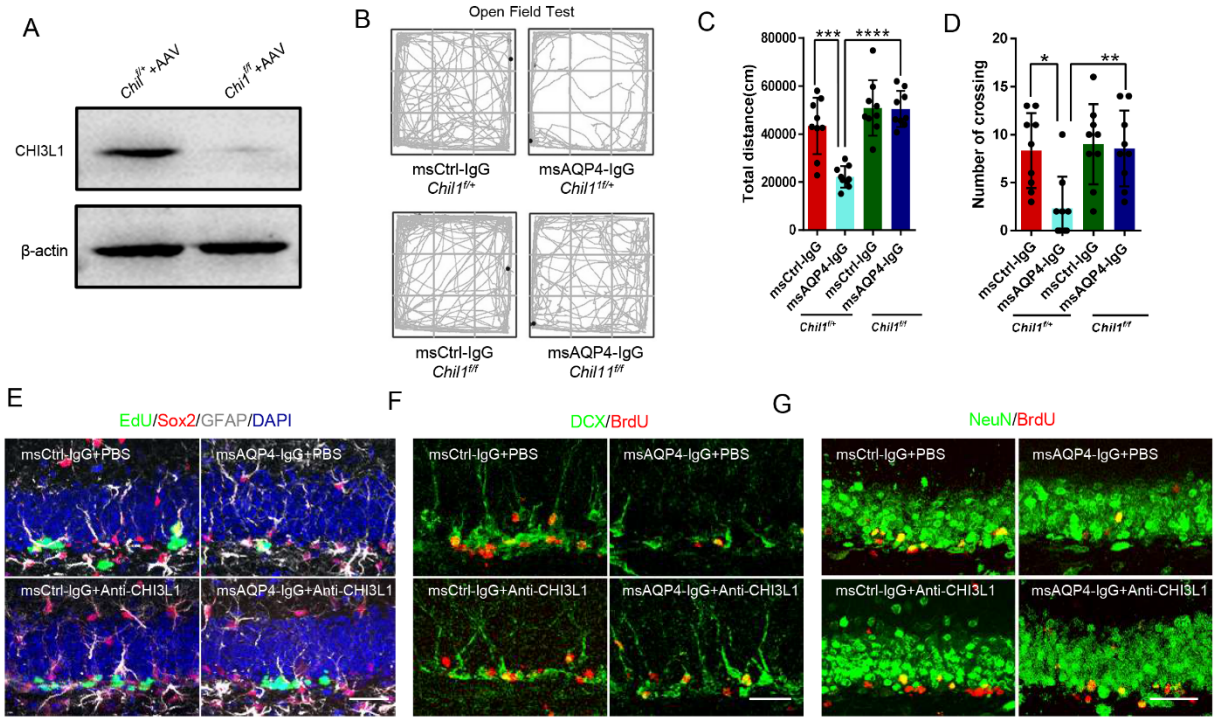

Fig. S6 Additional behavioral data for the effects of astrocyte-specific CHI3L1 knock out

(**A**) The evaluation of CHI3L1 knockout efficiency to complement **Fig. 6B and C**, by immunoblotting on the hippocampal lysates harvested from the *Chil1*$^{f/+}$ (control) or *Chil1*$^{f/f}$ (conditional knockout) mice receiving AAV injections for Cre-mediated CHI3L1 deletion.

(**B**) Related to **Fig. 6D-F**, the open filed test (OFT) was performed before the MWM experiments to assess the general locomotor activities and anxiety-like behaviors, with the representative movement paths from the t tested groups shown here: *Chil1*$^{f/+}$+msCtrl-IgG, *Chil1*$^{f/+}$+msAQP4-IgG, *Chil1*$^{f/f}$ +msCtrl-IgG and *Chil1*$^{f/f}$ +msAQP4-IgG.

(**C** and **D**) Quantification of the OPT results plotted as the total travelled distances (B) and the numbers of crossing over the center area (C) for the 4 groups. n=9 animal per group.

(**E**) Representative images to complement **Fig. 6M-O**, showing the mouse dentate gyrus sections labeled with EdU (green) and NSC markers Sox2 (red) and GFAP (gray). Scale bars, 50 μm.

(**F**) Representative images to complement **Fig. 6P**, showing the differentiation of BrdU-labeled NSCs into immature neurons, immunostained with BrdU (red) and DCX (green). Scale bars, 50 μm.

(**G**) Representative images to complement **Fig. 6Q**, showing the differentiation of BrdU-labeled NSCs into mature neurons, immunostained with BrdU (red) and NeuN (green). Scale bars, 50 μm.

Bar graphs were presented as the mean ± SEM and the statistical analyses were carried out with two-way ANOVA with Tukey's multiple comparisons test. Non-significant comparisons are not identified. *$p < 0.05$, **$p<0.01$, ***$p < 0.001$, ****$p < 0.001$.

Supplementary Figure 7

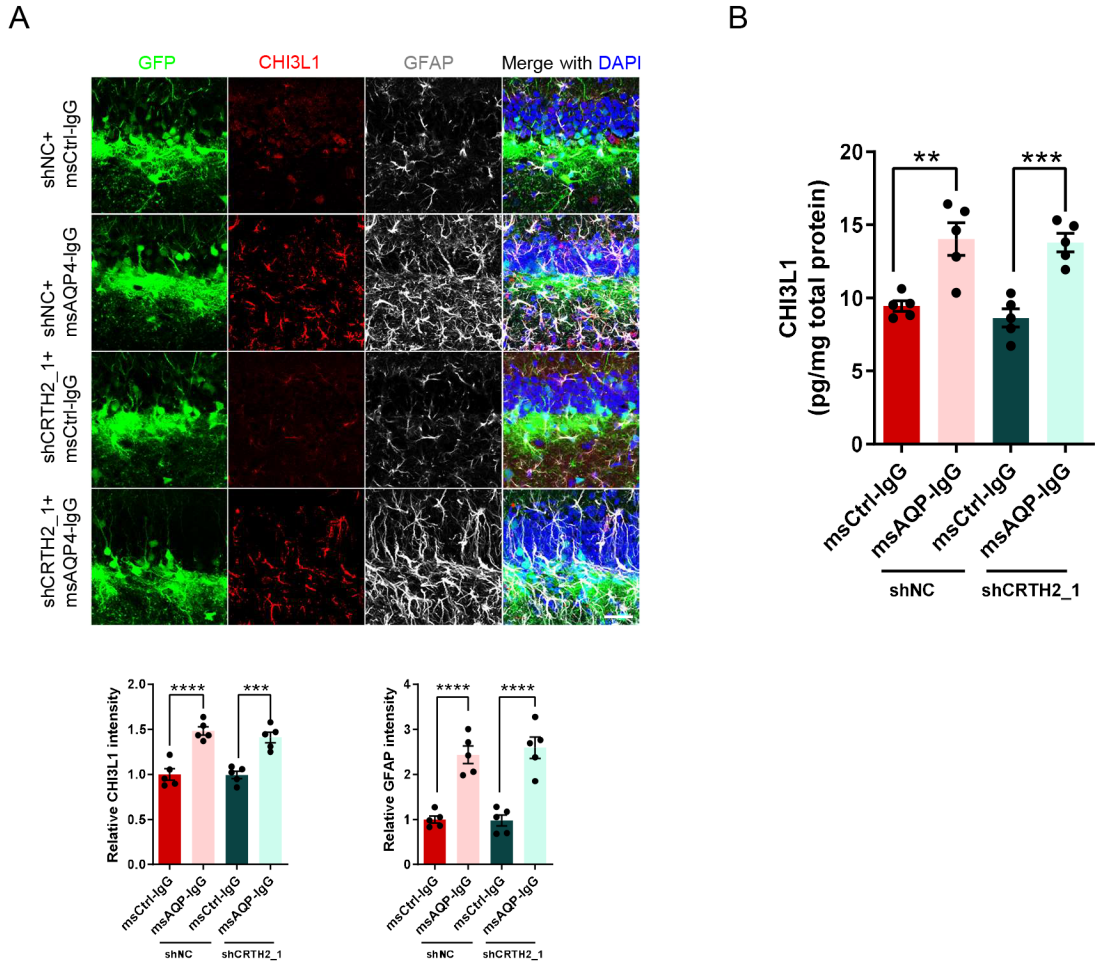

Fig. S7 The evaluation of astrocyte activation in mouse hippocampi infused with anti-AQP4 IgG or control IgG, with or without CRTH2 knockdown (complementing Fig. 7D-G).

(**A**) Representative images and confocal analyses of the mouse dentate gyrus sections from mice infused with msCtrl-IgG or msAQP4-IgG, plus stereotaxic injections of lentiviruses expressing eGFP together with a control shRNA (shCtrl) or the shRNA against CRTH2 (shCRTH2_1), and being sacrificed 4 weeks after the lentiviruses injections, as in **Fig. 7A**. Bar graphs of quantification of the immunofluorescent signals of CHI3L1 (red, left) and GFAP (gray, right), showing the astrocyte activation induced by msAQP4-IgG and no discernible change caused by the shRNA-mediated CRTH2 knockdown. n=5 animals per group. Scale bars, 50 μm.

(**B**) Measurements of CHI3L1 levels by ELISA on the lysates of acutely dissected, unfixed hippocampal tissues from the mouse brains. n=5 animals per group.

All data were presented as the mean ± SEM and the statistical significance was evaluated with one-way ANOVA and Tukey's post hoc multiple comparisons. Non-significant comparisons are not identified. *$p < 0.05$, **$p<0.01$, ***$p < 0.001$, ****$p < 0.001$.

Supplementary Table 1

Study	Groups	Number	Age (years, mean ± SEM)	Male / Female (n)	Serum AQP4-IgG, positive/negative	Disease duration	Mean EDSS scores	CHI3L1 in serum (ng/mL)	CHI3L1 in CSF (ng/mL)	*P*-value	Reference DOI
Correale et al.(*19*)	HCs	24	38.4 ± 4.3	16/8	-	-	-	-	73.7 ± 21.7	p<0.01	10.1177/1352458510392619
	NMO	12	38.0 ± 4.5	8/4	-	4.8 ± 2.1 (years)	3.7 ± 0.8	-	184 ± 18.4		
Qi et al.(*18*)	ONNDs	21	45.6 ± 19.0	16/5	-	-	-	-	117.1 ± 17.1	p<0.001	10.1016/j.msard.2020.102395
	NMO	29	45.9 ± 14.0	25/4	21/8	4.2 ± 5.4 (years)	4.3 ± 2.0	-	293.6 ± 33.9		
Cubas-Nunez et al.(*20*)	HCs	17	42 (35–50)	8/9	-	-	-	-	64.8 (47.4–78.3)	p< 0.001	10.1212/NXI.0000000000000972
	NMO	7	35 (31–36)	0/7	7/0	-	-	-	208.2 (111–448)		
Kaya et al. (*87*)	HCs	16	-	-	-	-	-	32.13±13.08	-	p<0.05	https://n.neurology.org/content/84/14_Supplement/P5.271
	NMO	26	-	-	-	-	-	66.71±66.71	-		
This study	HCs	46	41.3±9.0	23/23	-	-	-	25.2±9.4	95.5 ± 43.4	p< 0.001	-
	NMO	73	42.8±12.1	7/66	73/0	36.3 ± 14.5 (months)	2.9 ± 1.8	47.7±28.0	143.8 ± 54.2		

Table S1 The summary of prior clinical studies on CHI3L1 levels in NMO patients.

Abbreviations: HCs, healthy controls. NMO, neuromyelitis optica patients. ONNDs, control subjects with non-inflammatory neurological disorders. EDSS, Kurtzke Expanded Disability Status Scale, ranging from 0-10; the first levels 1.0 to 4.5 refer to people with a higher degree of ambulatory ability and the subsequent levels 5.0 to 9.5 refer to the loss of ambulatory ability.

Supplementary Table 2

	NMO patients (Serum)	HCs (Serum)	P-value	NMO patients (CSF)	HCs (CSF)	P-value
Age, years (range)	43.2± 13.4	38.6±7.1	0.1586	42.1±9.9	43.4±9.7	0.6369
Men/Women (n)	4/40	9/11	0.0019	3/26	14/12	0.0010
Years of education	10.2± 6.2	12.0 ± 4.3	0.2557	10.7±4.5	10.3±4.5	0.7207
AQP4-Ab, positive/negative	44/0	-	-	29/0	-	-
Disease duration (months)	41.0 ± 12.1	-	-	29.2 ± 15.1	-	-
Mean EDSS scores	3.1 ± 2.1	-	-	2.6 ± 1.0	-	-
Brain lesions (n)	27/44	-	-	22/29	-	-
Optic neuritis lesions (n)	36/44	-	-	18/29	-	-
Myelitis lesions (n)	22/44	-	-	15/29	-	-

Table S2 The clinical characteristics and demography of health controls and NMO patients enrolled for analyses of serum CHI3L1 levels or CSF CHI3L1 levels.

For measurements of CHI3L1 levels, the serum samples from 20 healthy controls (HCs) and 44 neuromyelitis optica (NMO) patients were used, and the CSF samples from additional 26 HCs and 29 NMO were used. Data are presented as the mean ± SEM.

Abbreviations: AQP4-Ab, the presence of aquaporin-4 autoantibody in the serum. EDSS, Kurtzke Expanded Disability Status Scale.

Supplementary Table 3

Patient	Sex	Age at onset (years)	Age at sampling	Serum AQP4-IgG	Clinical phenotype		Final diagnosis	Surgery
1	F	23	23	Positive	Relapsing	ON/ML/BR	NMO	Brain biopsy
2	F	24	25	Negative	N/A	N/A	Cerebral trauma	Brain biopsy

Table S3 Information regarding the biopsied brain samples from the control and NMO patient (complementary to Fig. 2B).
The further detailed information regarding these 2 subjects were reported in the prior studies, Luo *et al*., (*33*); Chang *et al*., (*49*).
Abbreviation: ON: optic neuritis, ML: myelitis, BR: brain lesion, NMO: neuromyelitis optica.

Data File 1

Data file S1 Raw numeric data and statistics for all figures presented in the main text and Supplementary Materials.

REFERENCES AND NOTES

1. T. Zhao, Z. Su, Y. Li, X. Zhang, Q. You, Chitinase-3 like-protein-1 function and its role in diseases. *Signal Transduct. Target. Ther.* **5**, 201 (2020).

2. K. Connolly, M. Lehoux, R. O'Rourke, B. Assetta, G. A. Erdemir, J. A. Elias, C. G. Lee, Y.-W. A. Huang, Potential role of chitinase-3-like protein 1 (CHI3L1/YKL-40) in neurodegeneration and Alzheimer's disease. *Alzheimers Dement.* **19**, 9–24 (2023).

3. C. G. Lee, C. A. Da Silva, C. S. Dela Cruz, F. Ahangari, B. Ma, M. J. Kang, C. H. He, S. Takyar, J. A. Elias, Role of chitin and chitinase/chitinase-like proteins in inflammation, tissue remodeling, and injury. *Annu. Rev. Physiol.* **73**, 479–501 (2011).

4. S. Kamle, B. Ma, C. H. He, B. Akosman, Y. Zhou, C.-M. Lee, W. S. El-Deiry, K. Huntington, O. Liang, J. T. Machan, M.-J. Kang, H. J. Shin, E. Mizoguchi, C. G. Lee, J. A. Elias, Chitinase 3-like-1 is a therapeutic target that mediates the effects of aging in COVID-19. *JCI Insight* **6**, e148749 (2021).

5. E. J. Kwak, J. Y. Hong, M. N. Kim, S. Y. Kim, S. H. Kim, C. O. Park, K. W. Kim, C. G. Lee, J. A. Elias, H. M. Jee, M. H. Sohn, Chitinase 3-like 1 drives allergic skin inflammation via Th2 immunity and M2 macrophage activation. *Clin. Exp. Allergy* **49**, 1464–1474 (2019).

6. C. G. Lee, D. Hartl, G. R. Lee, B. Koller, H. Matsuura, C. A. Da Silva, M. H. Sohn, L. Cohn, R. J. Homer, A. A. Kozhich, A. Humbles, J. Kearley, A. Coyle, G. Chupp, J. Reed, R. A. Flavell, J. A. Elias, Role of breast regression protein 39 (BRP-39)/chitinase 3-like-1 in Th2 and IL-13-induced tissue responses and apoptosis. *J. Exp. Med.* **206**, 1149–1166 (2009).

7. C.-M. Lee, C. H. He, A. M. Nour, Y. Zhou, B. Ma, J. W. Park, K. H. Kim, C. Dela Cruz, L. Sharma, M. L. Nasr, Y. Modis, C. G. Lee, J. A. Elias, IL-13Rα2 uses TMEM219 in chitinase 3-like-1-induced signalling and effector responses. *Nat. Commun.* **7**, 12752 (2016).

8. D. Low, R. Subramaniam, L. Lin, T. Aomatsu, A. Mizoguchi, A. Ng, A. K. DeGruttola, C. G. Lee, J. A. Elias, A. Andoh, M. Mino-Kenudson, E. Mizoguchi, Chitinase 3-like 1 induces survival and proliferation of intestinal epithelial cells during chronic inflammation and colitis-associated cancer by regulating S100A9. *Oncotarget* **6**, 36535–36550 (2015).

9. H. T. Tran, I. A. Lee, D. Low, A. Kamba, A. Mizoguchi, H. N. Shi, C. G. Lee, J. A. Elias, E. Mizoguchi, Chitinase 3-like 1 synergistically activates IL6-mediated STAT3 phosphorylation in intestinal epithelial cells in murine models of infectious colitis. *Inflamm. Bowel Dis.* **20**, 835–846 (2014).

10. Y. Zhou, H. Peng, H. Sun, X. Peng, C. Tang, Y. Gan, X. Chen, A. Mathur, B. Hu, M. D. Slade, R. R. Montgomery, A. C. Shaw, R. J. Homer, E. S. White, C. M. Lee, M. W. Moore, M. Gulati, C. G. Lee, J. A. Elias, E. L. Herzog, Chitinase 3-like 1 suppresses injury and promotes fibroproliferative responses in mammalian lung fibrosis. *Sci. Transl. Med.* **6**, 240ra276 (2014).

11. B. V. Lananna, C. A. McKee, M. W. King, J. L. Del-Aguila, J. M. Dimitry, F. H. G. Farias, C. J. Nadarajah, D. D. Xiong, C. Guo, A. J. Cammack, J. A. Elias, J. Zhang, C. Cruchaga, E. S. Musiek, Chi3l1/YKL-40 is controlled by the astrocyte circadian clock and regulates neuroinflammation and Alzheimer's disease pathogenesis. *Sci. Transl. Med.* **12**, eaax3519 (2020).

12. L. Li, E. Tian, X. Chen, J. Chao, J. Klein, Q. Qu, G. Sun, G. Sun, Y. Huang, C. D. Warden, P. Ye, L. Feng, X. Li, Q. Cui, A. Sultan, P. Douvaras, V. Fossati, N. E. Sanjana, A. D. Riggs, Y. Shi, GFAP mutations in astrocytes impair oligodendrocyte progenitor proliferation and myelination in an hiPSC model of Alexander disease. *Cell Stem Cell* **23**, 239–251.e6 (2018).

13. J. Wurm, S. P. Behringer, V. M. Ravi, K. Joseph, N. Neidert, J. P. Maier, R. Doria-Medina, M. Follo, D. Delev, D. Pfeifer, J. Beck, R. Sankowski, O. Schnell, D. H. Heiland, Astrogliosis releases pro-oncogenic chitinase 3-like 1 causing MAPK signaling in glioblastoma. *Cancers (Basel)* **11**, 1437 (2019).

14. P. Muszynski, M. Groblewska, A. Kulczynska-Przybik, A. Kulakowska, B. Mroczko, YKL-40 as a potential biomarker and a possible target in therapeutic strategies of Alzheimer's disease. *Curr. Neuropharmacol.* **15**, 906–917 (2017).

15. C. L. Sutphen, M. S. Jasielec, A. R. Shah, E. M. Macy, C. Xiong, A. G. Vlassenko, T. L. Benzinger, E. E. Stoops, H. M. Vanderstichele, B. Brix, H. D. Darby, M. L. Vandijck, J. H. Ladenson, J. C. Morris, D. M. Holtzman, A. M. Fagan, Longitudinal cerebrospinal fluid biomarker changes in preclinical Alzheimer disease during middle age. *JAMA Neurol.* **72**, 1029–1042 (2015).

16. F. M. Iwamoto, A. F. Hottinger, S. Karimi, E. Riedel, J. Dantis, M. Jahdi, K. S. Panageas, A. B. Lassman, L. E. Abrey, M. Fleisher, L. M. DeAngelis, E. C. Holland, A. Hormigo, Serum YKL-40 is a marker of prognosis and disease status in high-grade gliomas. *Neuro Oncol.* **13**, 1244–1251 (2011).

17. S. Floro, T. Carandini, A. M. Pietroboni, M. A. De Riz, E. Scarpini, D. Galimberti, Role of chitinase 3-like 1 as a biomarker in multiple sclerosis: A systematic review and meta-analysis. *Neurol. Neuroimmunol. Neuroinflamm.* **9**, e1164 (2022).

18. Y. Qi, L. S. Chou, L. J. Zhang, M. Q. Liu, M. Yi, Q. X. Zhang, J. Wang, T. Li, D. Q. Zhang, L. Yang, Increased cerebrospinal fluid YKL-40 levels are associated with disease severity of neuromyelitis optica spectrum disorders. *Mult. Scler. Relat. Disord.* **45**, 102395 (2020).

19. J. Correale, M. Fiol, Chitinase effects on immune cell response in neuromyelitis optica and multiple sclerosis. *Mult. Scler.* **17**, 521–531 (2011).

20. Y. Qi, L.-S. Chou, L.-J. Zhang, M.-Q. Liu, M. Yi, Q.-X. Zhang, J. Wang, T. Li, D.-Q. Zhang, L. Yang, Increased cerebrospinal fluid YKL-40 levels are associated with disease severity of neuromyelitis optica spectrum disorders. *Mult. Scler. Relat. Disord.* **45**, 102395 (2020).

21. L. Cubas-Núñez, S. Gil-Perotín, J. Castillo-Villalba, V. López, L. Solís Tarazona, R. Gasqué-Rubio, S. Carratalá-Boscá, C. Alcalá-Vicente, F. Pérez-Miralles, H. Lassmann, B. Casanova, Potential role of CHI3L1+ astrocytes in progression in MS. *Neurol. Neuroimmunol. Neuroinflamm.* **8**, e972 (2021).

22. V. A. Lennon, D. M. Wingerchuk, T. J. Kryzer, S. J. Pittock, C. F. Lucchinetti, K. Fujihara, I. Nakashima, B. G. Weinshenker, A serum autoantibody marker of neuromyelitis optica: Distinction from multiple sclerosis. *Lancet* **364**, 2106–2112 (2004).

23. D. Czarnecka, M. Oset, I. Karlinska, M. Stasiolek, Cognitive impairment in NMOSD—More questions than answers. *Brain Behav.* **10**, e01842 (2020).

24. E. Lopez-Soley, J. E. Meca-Lallana, S. Llufriu, Y. Blanco, R. Gomez-Ballesteros, J. Maurino, F. Perez-Miralles, L. Forero, C. Calles, M. L. Martinez-Gines, I. Gonzalez-Suarez, S. Boyero, L. Romero-Pinel, A. P. Sempere, V. Meca-Lallana, L. Querol, L. Costa-Frossard, M. Sepulveda, E. Solana, Cognitive

performance and health-related quality of life in patients with neuromyelitis optica spectrum disorder. *J. Pers. Med.* **12**, 743 (2022).

25. L. Cacciaguerra, P. Valsasina, A. Meani, G. C. Riccitelli, M. Radaelli, M. A. Rocca, M. Filippi, Volume of hippocampal subfields and cognitive deficits in neuromyelitis optica spectrum disorders. *Eur. J. Neurol.* **28**, 4167–4177 (2021).

26. F. Zheng, Y. Li, Z. Zhuo, Y. Duan, G. Cao, D. Tian, X. Zhang, K. Li, F. Zhou, M. Huang, H. Li, Y. Li, C. Zeng, N. Zhang, J. Sun, C. Yu, X. Han, S. Hallar, F. Barkhof, Y. Liu, Structural and functional hippocampal alterations in multiple sclerosis and neuromyelitis optica spectrum disorder. *Mult. Scler.* **28**, 707–717 (2022).

27. Y. Liu, Y. Fu, M. M. Schoonheim, N. Zhang, M. Fan, L. Su, Y. Shen, Y. Yan, L. Yang, Q. Wang, N. Zhang, C. Yu, F. Barkhof, F. D. Shi, Structural MRI substrates of cognitive impairment in neuromyelitis optica. *Neurology* **85**, 1491–1499 (2015).

28. W. Qiu, A. G. Kermode, Brain MRI in neuromyelitis optica: What is its role? *Curr. Neurol. Neurosci. Rep.* **11**, 526–528 (2011).

29. R. Li, C. Li, Z. Mao, Q. Huang, Y. Shu, Y. Chang, J. Wang, Y. Wang, W. Qiu, Male patients with neuromyelitis optica spectrum disorders: Different clinical characteristics and worse steroid treatment response. *Neurol. Sci.* **42**, 3267–3274 (2021).

30. M. L. Monje, S. Mizumatsu, J. R. Fike, T. D. Palmer, Irradiation induces neural precursor-cell dysfunction. *Nat. Med.* **8**, 955–962 (2002).

31. M. L. Monje, H. Toda, T. D. Palmer, Inflammatory blockade restores adult hippocampal neurogenesis. *Science* **302**, 1760–1765 (2003).

32. C. T. Ekdahl, J. H. Claasen, S. Bonde, Z. Kokaia, O. Lindvall, Inflammation is detrimental for neurogenesis in adult brain. *Proc. Natl. Acad. Sci. U.S.A.* **100**, 13632–13637 (2003).

33. B. Asrican, J. Wooten, Y. D. Li, L. Quintanilla, F. Zhang, C. Wander, H. Bao, C. Y. Yeh, Y. J. Luo, R. Olsen, S. A. Lim, J. Hu, P. Jin, J. Song, Neuropeptides modulate local astrocytes to regulate adult hippocampal neural stem cells. *Neuron* **108**, 349–366.e6 (2020).

34. W. Luo, H. Xu, L. Xu, W. Jiang, C. Chen, Y. Chang, C. Liu, Z. Tian, X. Qiu, C. Xie, X. Li, H. Chen, S. Lai, L. Wu, Y. Cui, C. Tang, W. Qiu, Remyelination in neuromyelitis optica spectrum disorder is promoted by edaravone through mTORC1 signaling activation. *Glia* **71**, 284–304 (2023).

35. C. Tang, M. Wang, P. Wang, L. Wang, Q. Wu, W. Guo, Neural stem cells behave as a functional niche for the maturation of newborn neurons through the secretion of PTN. *Neuron* **101**, 32–44.e6 (2019).

36. J. Wang, Y. Cui, Z. Yu, W. Wang, X. Cheng, W. Ji, S. Guo, Q. Zhou, N. Wu, Y. Chen, Y. Chen, X. Song, H. Jiang, Y. Wang, Y. Lan, B. Zhou, L. Mao, J. Li, H. Yang, W. Guo, X. Yang, Brain endothelial cells maintain lactate homeostasis and control adult hippocampal neurogenesis. *Cell Stem Cell* **25**, 754–767.e9 (2019).

37. S. R. Hinson, I. C. Clift, N. Luo, T. J. Kryzer, V. A. Lennon, Autoantibody-induced internalization of CNS AQP4 water channel and EAAT2 glutamate transporter requires astrocytic Fc receptor. *Proc. Natl. Acad. Sci. U.S.A.* **114**, 5491–5496 (2017).

38. M. E. Walker-Caulfield, Y. Guo, R. K. Johnson, C. B. McCarthy, P. D. Fitz-Gibbon, C. F. Lucchinetti, C. L. Howe, NFκB signaling drives pro-granulocytic astroglial responses to neuromyelitis optica patient IgG. *J. Neuroinflammation* **12**, 185 (2015).

39. C. L. Howe, T. Kaptzan, S. M. Magana, J. R. Ayers-Ringler, R. G. LaFrance-Corey, C. F. Lucchinetti, Neuromyelitis optica IgG stimulates an immunological response in rat astrocyte cultures. *Glia* **62**, 692–708 (2014).

40. K. Miyazaki-Komine, Y. Takai, P. Huang, O. Kusano-Arai, H. Iwanari, T. Misu, K. Koda, K. Mitomo, T. Sakihama, Y. Toyama, K. Fujihara, T. Hamakubo, M. Yasui, Y. Abe, High avidity chimeric monoclonal antibodies against the extracellular domains of human aquaporin-4 competing with the neuromyelitis optica autoantibody, NMO-IgG. *Br. J. Pharmacol.* **173**, 103–114 (2016).

41. P. Hasel, I. V. L. Rose, J. S. Sadick, R. D. Kim, S. A. Liddelow, Neuroinflammatory astrocyte subtypes in the mouse brain. *Nat. Neurosci.* **24**, 1475–1487 (2021).

42. K. A. Guttenplan, M. K. Weigel, D. I. Adler, J. Couthouis, S. A. Liddelow, A. D. Gitler, B. A. Barres, Knockout of reactive astrocyte activating factors slows disease progression in an ALS mouse model. *Nat. Commun.* **11**, 3753 (2020).

43. J. L. Zamanian, L. Xu, L. C. Foo, N. Nouri, L. Zhou, R. G. Giffard, B. A. Barres, Genomic analysis of reactive astrogliosis. *J. Neurosci.* **32**, 6391–6410 (2012).

44. W. Luo, G. Pant, Y. K. Bhavnasi, S. G. Blanchard, Jr., C. Brouwer, Pathview Web: User friendly pathway visualization and data integration. *Nucleic Acids Res.* **45**, W501–W508 (2017).

45. M. Kanehisa, The KEGG database. *Novartis Found. Symp.* **247**, 91–101 (2002).

46. A. Subramanian, P. Tamayo, V. K. Mootha, S. Mukherjee, B. L. Ebert, M. A. Gillette, A. Paulovich, S. L. Pomeroy, T. R. Golub, E. S. Lander, J. P. Mesirov, Gene set enrichment analysis: A knowledge-based approach for interpreting genome-wide expression profiles. *Proc. Natl. Acad. Sci. U.S.A.* **102**, 15545–15550 (2005).

47. S. A. Liddelow, B. A. Barres, Reactive astrocytes: Production, function, and therapeutic potential. *Immunity* **46**, 957–967 (2017).

48. H. Tang, Y. Sun, Z. Shi, H. Huang, Z. Fang, J. Chen, Q. Xiu, B. Li, YKL-40 induces IL-8 expression from bronchial epithelium via MAPK (JNK and ERK) and NF-κB pathways, causing bronchial smooth muscle proliferation and migration. *J. Immunol.* **190**, 438–446 (2013).

49. Y. Kim, S. Y. Kim, S.-M. Han, R. M. Payumo, K. Park, H. E. Kim, S.-H. Kim, J.-W. Hyun, E. Lee, H. J. Kim, Functional impairment of $CD19^{+}$ $CD24^{hi}$ $CD38^{hi}$ B cells in neuromyelitis optica spectrum disorder is restored by B cell depletion therapy. *Sci. Transl. Med.* **13**, eabk2132 (2021).

50. Y. Chang, W. Qiu, B. Zhang, D. He, H. Yang, Z. Lu, X. Hu, Analysis of two cases of Neuromyelitis Optica combined with tumefactive demyelinating lesions. *Chinese J. Neurol.* **47**, 163–167 2014).

51. W. Guo, N. E. Patzlaff, E. M. Jobe, X. Zhao, Isolation of multipotent neural stem or progenitor cells from both the dentate gyrus and subventricular zone of a single adult mouse. *Nat. Protoc.* **7**, 2005–2012 (2012).

52. C. H. He, C. G. Lee, C. S. Dela Cruz, C. M. Lee, Y. Zhou, F. Ahangari, B. Ma, E. L. Herzog, S. A. Rosenberg, Y. Li, A. M. Nour, C. R. Parikh, I. Schmidt, Y. Modis, L. Cantley, J. A. Elias, Chitinase 3-like 1 regulates cellular and tissue responses via IL-13 receptor α2. *Cell Rep.* **4**, 830–841 (2013).

53. C.-M. Lee, C. H. He, A. M. Nour, Y. Zhou, B. Ma, J. W. Park, K. H. Kim, C. Dela Cruz, L. Sharma, M. L. Nasr, Y. Modis, C. G. Lee, J. A. Elias, IL-13Rα2 uses TMEM219 in chitinase 3-like-1-induced signalling and effector responses. *Nat. Commun.* **7**, 12752 (2016).

54. B. Ma, S. Kamle, C. He, C. Lee, J. A. Elias, Inhibition of melanoma lung metastasis by Chi3l1 neutralizing antibody. *Am. J. Respir. Crit. Care Med.* **197**, A5944 (2018).

55. C. Geis, C. Ritter, C. Ruschil, A. Weishaupt, B. Grünewald, G. Stoll, T. Holmoy, T. Misu, K. Fujihara, B. Hemmer, C. Stadelmann, J. L. Bennett, C. Sommer, K. V. Toyka, The intrinsic pathogenic role of autoantibodies to aquaporin 4 mediating spinal cord disease in a rat passive-transfer model. *Exp. Neurol.* **265**, 8–21 (2015).

56. L.-W. Yick, O. K.-F. Ma, R. C.-L. Ng, J. S.-C. Kwan, K.-H. Chan, Aquaporin-4 autoantibodies from neuromyelitis optica spectrum disorder patients induce complement-independent immunopathologies in mice. *Front. Immunol.* **9**, 1438 (2018).

57. X. Zhao, H. van Praag, Steps towards standardized quantification of adult neurogenesis. *Nat. Commun.* **11**, 4275 (2020).

58. C. Tang, W. Guo, Implantation of a mini-osmotic pump plus stereotactical injection of retrovirus to study newborn neuron development in adult mouse hippocampus. *STAR Protoc.* **2**, 100374 (2021).

59. Y. Zhou, C. H. He, E. L. Herzog, X. Peng, C. M. Lee, T. H. Nguyen, M. Gulati, B. R. Gochuico, W. A. Gahl, M. L. Slade, C. G. Lee, J. A. Elias, Chitinase 3-like-1 and its receptors in Hermansky-Pudlak syndrome-associated lung disease. *J. Clin. Invest.* **125**, 3178–3192 (2015).

60. D. C. Lie, S. A. Colamarino, H. J. Song, L. Désiré, H. Mira, A. Consiglio, E. S. Lein, S. Jessberger, H. Lansford, A. R. Dearie, F. H. Gage, Wnt signalling regulates adult hippocampal neurogenesis. *Nature* **437**, 1370–1375 (2005).

61. L. Xue, S. L. Gyles, A. Barrow, R. Pettipher, Inhibition of PI3K and calcineurin suppresses chemoattractant receptor-homologous molecule expressed on Th2 cells (CRTH2)-dependent responses of Th2 lymphocytes to prostaglandin D(2). *Biochem. Pharmacol.* **73**, 843–853 (2007).

62. A. Krishnankutty, T. Kimura, T. Saito, K. Aoyagi, A. Asada, S.-I. Takahashi, K. Ando, M. Ohara-Imaizumi, K. Ishiguro, S.-I. Hisanaga, In vivo regulation of glycogen synthase kinase 3β activity in neurons and brains. *Sci. Rep.* **7**, 8602 (2017).

63. S. Ding, T. Y. Wu, A. Brinker, E. C. Peters, W. Hur, N. S. Gray, P. G. Schultz, Synthetic small molecules that control stem cell fate. *Proc. Natl. Acad. Sci. U.S.A.* **100**, 7632–7637 (2003).

64. D. H. Kim, H. J. Park, S. Lim, J. H. Koo, H. G. Lee, J. O. Choi, J. H. Oh, S. J. Ha, M. J. Kang, C. M. Lee, C. G. Lee, J. A. Elias, J. M. Choi, Regulation of chitinase-3-like-1 in T cell elicits Th1 and cytotoxic responses to inhibit lung metastasis. *Nat. Commun.* **9**, 503 (2018).

65. R. Pettipher, T. T. Hansel, R. Armer, Antagonism of the prostaglandin D2 receptors DP1 and CRTH2 as an approach to treat allergic diseases. *Nat. Rev. Drug Discov.* **6**, 313–325 (2007).

66. T. Luker, R. Bonnert, S. Brough, A. R. Cook, M. R. Dickinson, I. Dougall, C. Logan, R. T. Mohammed, S. Paine, H. J. Sanganee, C. Sargent, J. A. Schmidt, S. Teague, S. Thom, Substituted indole-1-acetic acids as potent and selective CRTh2 antagonists-discovery of AZD1981. *Bioorg. Med. Chem. Lett.* **21**, 6288–6292 (2011).

67. E. D. Bateman, C. O'Brien, P. Rugman, S. Luke, S. Ivanov, M. Uddin, Efficacy and safety of the CRTh2 antagonist AZD1981 as add-on therapy to inhaled corticosteroids and long-acting β(2)-agonists in patients with atopic asthma. *Drug Des. Devel. Ther.* **12**, 1093–1106 (2018).

68. C. S. Malo, R. H. Khadka, K. Ayasoufi, F. Jin, J. E. AbouChehade, M. J. Hansen, R. Iezzi, K. D. Pavelko, A. J. Johnson, Immunomodulation mediated by anti-angiogenic therapy improves CD8 T cell immunity against experimental glioma. *Front. Oncol.* **8**, 320 (2018).

69. E. Quintana, C. Coll, J. Salavedra-Pont, M. Munoz-San Martin, R. Robles-Cedeno, J. Tomas-Roig, M. Buxo, C. Matute-Blanch, L. M. Villar, X. Montalban, M. Comabella, H. Perkal, J. Gich, L. Ramio-Torrenta, Cognitive impairment in early stages of multiple sclerosis is associated with high cerebrospinal fluid levels of chitinase 3-like 1 and neurofilament light chain. *Eur. J. Neurol.* **25**, 1189–1191 (2018).

70. J. S. Snyder, N. Kee, J. M. Wojtowicz, Effects of adult neurogenesis on synaptic plasticity in the rat dentate gyrus. *J. Neurophysiol.* **85**, 2423–2431 (2001).

71. C. O. Lacefield, V. Itskov, T. Reardon, R. Hen, J. A. Gordon, Effects of adult-generated granule cells on coordinated network activity in the dentate gyrus. *Hippocampus* **22**, 106–116 (2012).

72. A. Marín-Burgin, L. A. Mongiat, M. B. Pardi, A. F. Schinder, Unique processing during a period of high excitation/inhibition balance in adult-born neurons. *Science* **335**, 1238–1242 (2012).

73. A. Bakker, C. B. Kirwan, M. Miller, C. E. L. Stark, Pattern separation in the human hippocampal CA3 and dentate gyrus. *Science* **319**, 1640–1642 (2008).

74. H. Abe, T. Takeshita, K. Nagata, T. Arita, Y. Endo, T. Fujita, H. Takayama, M. Kubo, K. Sugamura, Molecular cloning, chromosome mapping and characterization of the mouse CRTH2 gene, a putative member of the leukocyte chemoattractant receptor family. *Gene* **227**, 71–77 (1999).

75. T. Satoh, R. Moroi, K. Aritake, Y. Urade, Y. Kanai, K. Sumi, H. Yokozeki, H. Hirai, K. Nagata, T. Hara, M. Utsuyama, K. Hirokawa, K. Sugamura, K. Nishioka, M. Nakamura, Prostaglandin D2 plays an essential role in chronic allergic inflammation of the skin via CRTH2 receptor. *J. Immunol.* **177**, 2621–2629 (2006).

76. I. Spik, C. Brénuchon, V. Angéli, D. Staumont, S. Fleury, M. Capron, F. Trottein, D. Dombrowicz, Activation of the prostaglandin D2 receptor DP2/CRTH2 increases allergic inflammation in mouse. *J. Immunol.* **174**, 3703–3708 (2005).

77. R. Haba, N. Shintani, Y. Onaka, T. Kanoh, H. Wang, R. Takenaga, A. Hayata, H. Hirai, K. Y. Nagata, M. Nakamura, A. Kasai, R. Hashimoto, K. Nagayasu, T. Nakazawa, H. Hashimoto, A. Baba, Central

CRTH2, a second prostaglandin D2 receptor, mediates emotional impairment in the lipopolysaccharide and tumor-induced sickness behavior model. *J. Neurosci.* **34**, 2514–2523 (2014).

78. H. Hirai, K. Tanaka, O. Yoshie, K. Ogawa, K. Kenmotsu, Y. Takamori, M. Ichimasa, K. Sugamura, M. Nakamura, S. Takano, K. Nagata, Prostaglandin D2 selectively induces chemotaxis in T helper type 2 cells, eosinophils, and basophils via seven-transmembrane receptor CRTH2. *J. Exp. Med.* **193**, 255–262 (2001).

79. M. S. Abdel-Halim, I. Lunden, G. Cseh, E. Änggård, Prostaglandin profiles in nervous tissue and blood vessels of the brain of various animals. *Prostaglandins* **19**, 249–258 (1980).

80. H. Nango, Y. Kosuge, N. Yoshimura, H. Miyagishi, T. Kanazawa, K. Hashizaki, T. Suzuki, K. Ishige, The molecular mechanisms underlying Prostaglandin D_2-induced neuritogenesis in motor neuron-like NSC-34 cells. *Cells* **9**, 934 (2020).

81. S. Ghosh, A. M. Elder, K. G. Carson, K. Sprott, S. Harrison, PGD2 receptor antagonists for the treatment of inflammatory diseases. World Patent WO2004032848 (2004).

82. L. Corradini, M. J. Field, R. A Kinloch, B. I. Williams-Jones, Method of treating neuropathic pain using a CRTH2 receptor antagonist. World Patent WO2005102338 (2005).

83. S. H. Choi, R. E. Tanzi, Is Alzheimer's disease a neurogenesis disorder? *Cell Stem Cell* **25**, 7–8 (2019).

84. B. W. Dulken, M. T. Buckley, P. Navarro Negredo, N. Saligrama, R. Cayrol, D. S. Leeman, B. M. George, S. C. Boutet, K. Hebestreit, J. V. Pluvinage, T. Wyss-Coray, I. L. Weissman, H. Vogel, M. M. Davis, A. Brunet, Single-cell analysis reveals T cell infiltration in old neurogenic niches. *Nature* **571**, 205–210 (2019).

85. L. K. Smith, Y. He, J. S. Park, G. Bieri, C. E. Snethlage, K. Lin, G. Gontier, R. Wabl, K. E. Plambeck, J. Udeochu, E. G. Wheatley, J. Bouchard, A. Eggel, R. Narasimha, J. L. Grant, J. Luo, T. Wyss-Coray, S. A. Villeda, β2-microglobulin is a systemic pro-aging factor that impairs cognitive function and neurogenesis. *Nat. Med.* **21**, 932–937 (2015).

86. D. M. Wingerchuk, B. Banwell, J. L. Bennett, P. Cabre, W. Carroll, T. Chitnis, J. de Seze, K. Fujihara, B. Greenberg, A. Jacob, S. Jarius, M. Lana-Peixoto, M. Levy, J. H. Simon, S. Tenembaum, A. L. Traboulsee, P. Waters, K. E. Wellik, B. G. Weinshenker; International Panel for NMO Diagnosis, International consensus diagnostic criteria for neuromyelitis optica spectrum disorders. *Neurology* **85**, 177–189 (2015).

87. Y.-W. A. Huang, B. Zhou, A. M. Nabet, M. Wernig, T. C. Sudhof, Differential signaling mediated by ApoE2, ApoE3, and ApoE4 in human neurons parallels Alzheimer's disease risk. *J. Neurosci.* **39**, 7408–7427 (2019).

88. Y.-W. A. Huang, B. Zhou, M. Wernig, T. C. Sudhof, ApoE2, ApoE3, and ApoE4 differentially stimulate APP transcription and Aβ secretion. *Cell* **168**, 427–441.e21 (2017).

89. D. Kaya, Z. Altun, E. Idiman, N. Karabay, S. Cevik, D. Arslan, Serum chitinase 3-like 1 levels in patients with multiple sclerosis and neuromyelitis optica (P5.271). *Neurology* **84**, P5.271 (2015).